Eocene magmatism in the Himalaya: A response to lithospheric flexure during early Indian collision?

Lin Ma[1, 2, 3, 4]*, Qiang Wang[1, 3, 4]*, Andrew C. Kerr[2], Zheng-Xiang Li[5], Wei Dan[1, 3, 4], Ya-Nan Yang[1, 3], Jin-Sheng Zhou[1], Jun Wang[1], Cheng Li[1, 4]

[1] State Key Laboratory of Isotope Geochemistry, Guangzhou Institute of Geochemistry, Chinese Academy of Sciences, Guangzhou 510640, China

[2] School of Earth and Environmental Sciences, Cardiff University, Cardiff, Wales CF10 3AT, United Kingdom

[3] Excellent Centre for Deep Earth Sciences, Chinese Academy of Sciences, Guangzhou 510640, China

[4] College of Earth and Planetary Sciences, University of Chinese Academy of Sciences, Beijing 100049, China

[5] Earth Dynamics Research Group, TIGeR, School of Earth and Planetary Sciences, Curtin University, Perth, Western Australia, Australia

*Corresponding author. E-mail: malin@gig.ac.cn (L. Ma), wqiang@gig.ac.cn (Q. Wang)

Eocene mafic magmatism in the Himalaya provides a crucial window for probing the evolution of crustal anatexis processes within the lower-plate in a collisional orogen. Here we report geochemical data from the earliest post-collision ocean island basalt-like mafic dikes intruding the Tethyan Himalaya near the northern edge of the colliding Indian plate. These dikes occurred coevally, and spatially overlap with, Eocene granitoids in the cores of gneiss domes and are likely derived from interaction of melts from the lithosphere-asthenosphere boundary with the Indian continental lithosphere. We propose that these mafic magmas were emplaced along lithospheric fractures in response to lithospheric flexure during initial subduction of the Indian continent and that the underplating of such mafic magmas resulted in orogen-parallel crustal anatexis within the Indian continent. This mechanism can explain the formation of coeval magmatism and the geological evolution of collisional orogen on both sides of the suture zone.

INTRODUCTION

The Himalaya belt is the most active collisional orogen in the world. It exposes the former passive margins of the Indian continent, and it is characterized by widespread Cenozoic crustal anatexis, high-grade metamorphism and some orogen-scale normal and strike-slip faulting (Harrison et al., 1997; Yin, 2006) (Fig. 1a). These magmatic and metamorphic units distributed parallel to the suture within the lower plate/previously passive side of the collisional orogen, can yield significant information on the collision and related crustal reworking processes (Hou et al., 2012; Vanderhaeghe and Teyssier, 2001; Wang et al., 2021; Weller et al., 2021; Zeng et al., 2011).

Two critical episodes of Cenozoic metamorphism and magmatism have been identified from the Himalaya: 1) 48–35 Ma Barrovian-type prograde metamorphism with Eocene mafic and Na-rich adakitic melts (e.g., Hou et al., 2012; Ji et al., 2016), and 2) Late Oligocene–Early Miocene retrograde metamorphism associated with leucogranite formation (Harrison et al., 1997; Vanderhaeghe and Teyssier, 2001; Weller et al., 2021) (Fig. 1).

Himalayan uplift and associated crustal anatexis (Hou et al., 2012) has been linked to a range of possible processes including thin-skinned thrusting (DeCelles et al., 2002; Yin, 2006), middle-crustal melting and ductile flow (Nelson et al.,1996; Vanderhaeghe and Teyssier, 2001), or extrusion of an Indian crustal wedge (Chemenda et al., 2000). A variety of anatexis mechanisms beneath the Himalayas have been proposed, including: shear heating (Harrison et al., 1998), decompression melting (Davidson et al., 2008), radiogenic heating (Searle et al., 2003) and heat transferred from mantle-derived melts (Zheng et al., 2016). However, the links between the crustal anatexis event(s) and coeval tectonic developments remain unclear (Guo and Wilson, 2012; Hou et al., 2012 and references therein).

In this paper we report geochemical data from Eocene mafic dikes found in the Tethyan Himalaya that have ocean island basalt (OIB)-like compositions. This mafic magmatism occurred coevally, and spatially overlaps with, the well-developed Tethyan Himalayan granitoids and associated metamorphic event (Hou et al., 2012) (Fig. 1a-b). These dikes provide a rare opportunity to examine the origin of such enigmatic intraplate magmatism and related geodynamic evolution along the margin of the lower plate in a continental collision zone. Similar magmatism is also reported in other collisional orogens (Vanderhaeghe et al., 2020; Weller et al., 2021) and in this study we present a new geodynamic model for such orogen-parallel lower-plate magmatic and metamorphic belts.

BACKGROUND AND SAMPLES

The Himalaya-Tibet orogen was formed by the collision of the Indian continent with Eurasia that started along the Yarlung Zangbo Suture (YZS) (Fig. 1). The Lhasa block, immediately north of the YZS, represents the southern edge of the Asian upper plate, and experienced long-lived subduction of Neo-Tethyan ocean crust with extensive late Triassic to Eocene calc-alkaline plutonism and volcanism before the terminal collision (Zhu et al., 2013, 2019). Following the collision and a magmatic flare-up with a peak of 51 ± 3 Ma, arc magmatism in southern Tibet waned, as cold Indian lithosphere underthrust Tibet (Chung et al., 2005; Zhu et al., 2019).

On the opposite side of the suture is the lower Indian plate representing a pre-collisional stable craton, with slightly younger (ca. 48–35 Ma) high Sr/Y granitoids and limited OIB-type gabbros and medium-temperature eclogite–high pressure (EHP) granulite metamorphism (Fig. 1; Hou et al., 2012; Ji et al., 2016; Weller et al., 2021; Zeng et al., 2011). The high Sr/Y granitoids are believed to have derived from partial melting of amphibolite at ~880°C and ~10 kbar (Hou et al., 2012; Zeng et al., 2011). The 45 Ma Langshan gabbro, on the other hand, has HIMU (high μ, $\mu = {}^{238}U/{}^{204}Pb$)-type OIB signatures with depleted Sr-Nd isotopes. These gabbros are thought to have been generated by partial melting of the asthenosphere during detachment of the subducted Neo-Tethyan slab (Ji et al., 2016). Subsequent to this magmatic episode, kilometer-scale Himalayan leucogranite bodies (~25–15 Ma and ~8 Ma) were emplaced in the northern Himalaya (Fig. 1; Vanderhaeghe and Teyssier, 2001; Weller et al., 2021). These leucogranites were produced by muscovite-dehydration melting of meta-sediments (Weinberg, 2016) at ultrahigh temperature (UHT) conditions (900–970°C and 6–11 kbar [~40°C /km]), mostly between 25 and 15 Ma (Wang et al., 2021).

Several ENE-trending, broadly orogen-parallel, 5–8 m wide diabase dikes that intrude the Early Jurassic Ridang Formation limestone, marl limestone and shale, have recently been discovered near Gyangze (Figs. 1 and DR2). These dikes are coarse-grained and consist of clinopyroxene, plagioclase and amphibolite with secondary chlorite and sericite.

GEOCHRONOLOGY AND GEOCHEMISTRY

Zircon grains from the Gyantse diabase sample JZ18-2-1 yielded a U-Pb age of 48.6 ± 0.5 Ma (Fig. 2d, methodology and detailed analytical results in the Data Repository), that is slightly older than the Langshan OIB-type gabbro (45 ± 1.4 Ma, Ji et al., 2016) but overlaps with the earliest Cenozoic high Sr/Y granitoids (ca. 48–45 Ma; e.g., Hou et al., 2012). Zircon $\delta^{18}O$ values ranging from 5.1‰ to 6.4‰ with a mean of 5.9 ± 0.6‰, are consistent (within error) with mantle zircon values (5.3 ± 0.6‰).

The Gyantse diabase dikes have relatively broad ranges of SiO_2 (46.0 to 54.5 wt.%) and MgO (5.0 to 12.4 wt.%) contents, and plot in the field of alkali basaltic rocks (Fig. 2a). They have OIB-like element patterns with enriched Nb (11.4–21.5 ppm) and TiO_2 (1.9–2.9 wt.%) and a slight Eu anomaly (chondrite normalized $Eu/\sqrt[2]{Sm \times Gd} = 0.85 - 1.10$). Initial Sr-isotope ratios (0.7076–0.7115) and $\varepsilon_{Nd}(t)$ (−2.7 to −2.0), are more enriched than the Langshan gabbro but less so than the coeval granitoids (Fig. 2c).

PETROGENESIS AND GEOTECTONIC IMPLICATIONS

The Gyantse mafic dikes have relatively low Nb (11.7–21.5 ppm) and more enriched Sr-Nd isotope compositions than the Langshan gabbro which was likely formed by partial melting of asthenosphere (Ji et al., 2016), that contained more-enriched components. Given the insignificant crustal contamination of the Gyantse mafic magmas (see details in Data Repository), the Indian lithospheric mantle (Shellnutt et al., 2014) is the most likely source of this enriched component. Our modeling indicates that the Gyantse mafic dikes were most likely derived from the lithosphere-asthenosphere boundary (LAB) melts at the top of the asthenosphere with a contribution from the Indian lithospheric mantle (Figs. 2c and DR3). Seismic profiles show that the present depth of the LAB below eastern Himalaya ranges from 140 km to 100 km (Zhao et al. 2010), which is likely to be similar to, or greater than, the lithosphere thickness at the early stage of the collision (~50 Ma). Peridotite with 1.0–2.5 wt.% CO_2 or 200–300 ppm H_2O can produce stable partial melts at 3 Gpa (Hirschmann et al., 2009). The LAB has recently been documented to be volatile enriched (Blatter et al. 2022), and thus provides the most likely source for mafic magmas in Tethyan Himalaya during early collision.

The Early Eocene (51–45 Ma) magmatism, dominated by crustal anatexis, occurred on both sides of the YZS during early collision. The southern margin of Asian plate is characterized by thickened juvenile crust and a relatively high crustal thermal state (Ma et al., 2017). In contrast, the northern edge of the Indian plate is marked by a thickened ancient crust with a moderate geothermal gradient during the early stage of collision (Hou et al., 2012; Weller et al., 2021 and references therein). The 48–35 Ma Tethyan Himalaya magmatism, consisting of high Sr/Y granitoids within gneiss dome and coeval gabbros and dikes, is slightly younger than the magmatic peak in the Lhasa block (51±3 Ma) (Fig. 1). After that, another episode (25–8 Ma) of crustal anatexis of accreted sediments dominated the melting in the Himalaya (Guo and Wilson, 2012; Weller et al., 2021).

The sources of the two episodes of crustal anatexis along the northern Indian continental margin (one at around 48–35 Ma, and the other around 25–8 Ma) may be very different. The Miocene crustal anatexis accompanied by ultrahigh temperature (900–970 °C) metamorphism indicates a hotter crustal thermal state than the Eocene crustal anatexis events with moderate temperature (~600–750 °C) metamorphism (e.g., Wang et al., 2021; Weller et al., 2021). Numerous studies over the past few decades have been carried out on the Miocene crustal anatexis and related process, which led to the Cenozoic rise of the Himalaya orogen (Chemenda et al., 2000; DeCelles et al., 2002; Harrison et al., 1998; Nelson et al.,1996; Yin, 2006; Wang et al., 2021). However, the Eocene crustal anatexis event is poorly understood due to the lack of critical evidence. A previous model for the generation of mafic magmas in Tethyan Himalaya involves decompression melting of the asthenosphere triggered by the break-off of the Neo-Tethyan lithosphere (e.g., Ji et al., 2016). However, such a model has difficulties in accounting for the following geological observations. 1) Similar OIB-like magma has not been found in the Lhasa terrane below which the break-off of the Neo-Tethyan lithosphere is proposed to have occurred. 2) It would have been extremely difficult for OIB-like magma to migrate southwards from beneath the Lhasa terrane and emplace as the Indian plate continued to push northward against Eurasia. An alternative model is therefore required to reconcile coeval metamorphic and magmatic records and geological observations along both sides of the suture zone in this collisional orogen.

It has been noted that a sudden increase in the convergence rate of the Indian continent toward Eurasia occurred prior to its initial collision with Eurasia was likely a response to enhanced pull caused by the steepening subduction of the Neo-Tethyan plate (Fig. 3; Chung et al., 2005). Such a steepening of subduction may also have resulted in the likely steep geometry of the early subduction of the Indian continental margin (Qi et al., 2020). This steepening Neo-Tethyan and Indian lithospheric subduction may also have triggered subduction channel widening and asthenospheric upwelling under the southern Lhasa terrane (Kelly et al., 2019). This would have eventually resulted in break-off of the Neo-Tethyan oceanic slab (Hou et al., 2012), and/or lithospheric delamination of southern Lhasa terrane (Qi et al., 2020), causing melting to produce the ca. 51 Ma magmatism in southern Lhasa block along the suture zone (Fig. 3).

We propose here that after the 51 Ma magmatic event, a lithospheric flexure formed along the northern Indian continent parallel to the suture, causing brittle cracking (i.e., bending-induced faults; Romeo and Álvarez-Gómez, 2018) and the 48–45 Ma melting in northern Himalaya (Fig. 3a). The lithospheric flexure could have resulted from either: 1) the break-off of the subducted Neo-Tethyan lithosphere at ca. 50 Ma (Fig. 3a), and the resultant buoyancy-induced upward bending of the leading edge of the Indian continental lithosphere; or 2) the slowdown of subduction along the leading-edge of the subducting Indian lithosphere at ca. 50 Ma due to the buoyancy of the Indian continental crust while the Indian plate was still continuously pushing northward. This is consistent with the rapid slowdown of the Indian continent's northward movement since 50 Ma (Fig. 1c, Cande et al., 2010). In addition, the loading caused by crustal thickening after the collision may also have contributed to lithospheric bending (Fig. 3a).

In our model, the melts derived by decompression melting of the LAB intruded to the shallow levels of the lithosphere along extensional fractures below neutral plane of the downwarped lithosphere (Fig. 3). Given the rapid thickening of the Indian continental crust during the early collision, the neutral plane of the bended lithosphere could have been close to or above the Moho, with shortening above the neutral plane mostly absorbed by the series of crust thrusting (Fig. 3a). The high buoyancy of volatile-rich LAB melts and potential thermal–mechanical–chemical erosion could have driven the migration of the LAB melts through the lithosphere (Spence and Turcotte, 1985). Emplacement of such mafic magmas may not only form the reported gabbros and mafic dikes which are now exhumed to the surface by kilometers of erosion, associated mafic underplating in the crust likely also provided the heat source for the formation of coeval (51–40 Ma) orogen-parallel crustal anatexis, and thus the orogen-parallel gneiss domes (Hou et al., 2012; Weller et al., 2021). After this 48–35 Ma magmatic event, the ongoing over-thrusting and crustal compression enabled the accumulation of radiogenic heat in the lower crust. This radiogenic decay resulted in an elevated geotherm and causing the subsequent larger-scale crustal anatexis during the Miocene (Fig. 1). However, discussion and modelling of this process is beyond the scope of the present paper.

Overall, our model provides new insights into the mechanisms of magma generation and orogenic evolution within the lower plate (a previous passive margin)-side of convergent orogens. Such mechanisms may also be appliable to converging oceanic lower plates, where explanations for the mechanism of orogen-parallel magmatism range from a mantle transition zone origin (Yang and Faccenda, 2020) to melts formed at the LAB due to either lithospheric flexure-related extension (e.g., Hirano et al., 2006; Pilet et al., 2016) or enhanced pull of the subducting plate (Dan et al., 2021). Elements of our model also share similarities to that of Yuan et al. (2010) proposed for the formation of Triassic granitoids in the eastern Songpan-Ganzi Fold Belt. Our model may also be applicable to magmatism along the passive side of other collisional orogens.

ACKNOWLEDGMENTS

We appreciate valuable suggestions of Prof. U. Schaltegger, Prof. D. Brown, Prof. B. White, Prof. A. Yin, Prof. O. Vanderhaeghe and an anonymous reviewer. We also thank Prof. Yin-De Jiang and Dr. Xiu-Zheng Zhang for beneficial discussions. Financial support was provided by the Second Tibetan Plateau Scientific Expedition and Research (2019QZKK0702), the National Natural Science Foundation of China (Nos. 42122022, 41872062 and 42021002). ZXL acknowledge support from the Australian Research Council (Laureate Fellowship grant FL150100133). This is contribution XXXXXX from GIGCAS.

Reference

Blatter, D., Naif, S., Key, K., and Ray, A., 2022, A plume origin for hydrous melt at the lithosphere–asthenosphere boundary: Nature, v. 604, no. 7906, p. 491-494.

Cande, S. C., Patriat, P., and Dyment, J., 2010, Motion between the Indian, Antarctic and African plates in the early Cenozoic: Geophysical Journal International, v. 183, no. 1, p. 127-149.

Chapman, J. B., and Kapp, P., 2017, Tibetan Magmatism Database: Geochemistry, Geophysics, Geosystems, v. 18, no. 11, p. 4229-4234.

Chemenda, A., and Burg, J.-P., 2000, Evolutionary model of the Himalaya-Tibet system: Geopoem based on new modelling, geological and geophysical data: Earth and Planetary Science Letters, v. 174, p. 397-409.

Chung, S. L., Chu, M. F., Zhang, Y., Xie, Y., Lo, C. H., Lee, T. Y., Lan, C. Y., Li, X., Zhang, Q., and Wang, Y., 2005, Tibetan tectonic evolution inferred from spatial and temporal variations in post-collisional magmatism: Earth-Science Reviews, v. 68, no. 3-4, p. 173-196.

Dan, W., Wang, Q., White, W. M., Li, X.-H., Zhang, X.-Z., Tang, G.-J., Ou, Q., Hao, L.-L., and Qi, Y., 2021, Passive-margin magmatism caused by enhanced slab-pull forces in central Tibet Geology, v. 49, p. 130–134.

Davidson, C., Grujic, D., Hollister, L., and Schmid, S., 2008, Metamorphic reactions related to decompression and synkinematic intrusion of leucogranite, High Himalayan Crystallines, Bhutan: Journal of Metamorphic Geology, v. 15, p. 593-612.

DeCelles, P. G., Robinson, D. M., and Zandt, G., 2002, Implications of shortening in the Himalayan fold‐thrust belt for uplift of the Tibetan Plateau: Tectonics, v. 21, no. 6, p. 12-11-12-25.

Harrison, T. M., Lovera, O. M., and Grove, M., 1997, New insights into the origin of two contrasting Himalayan granite belts: Geology, v. 25, no. 10, p. 899-902.

Hirano, N., Takahashi, E., Yamamoto, J., Abe, N., Ingle, S. P., Kaneoka, I., Hirata, T., Kimura, J.-I., Ishii, T., and Ogawa, Y., 2006, Volcanism in response to plate flexure: Science, v. 313, no. 5792, p. 1426-1428.

Hirschmann, M. M., Tenner, T., Aubaud, C., and Withers, A., 2009, Dehydration melting of nominally anhydrous mantle: The primacy of partitioning: Physics of the Earth and Planetary

Interiors, v. 176, no. 1-2, p. 54-68.

Hou, Z.-Q., Zheng, Y.-C., Zeng, L.-S., Gao, L.-E., Huang, K.-X., Li, W., Li, Q.-Y., Fu, Q., Liang, W., and Sun, Q.-Z., 2012, Eocene–Oligocene granitoids in southern Tibet: constraints on crustal anatexis and tectonic evolution of the Himalayan orogen: Earth and Planetary Science Letters, v. 349, p. 38-52.

Ji, W. Q., Wu, F. Y., Chung, S. L., Wang, X. C., Liu, C. Z., Li, Q. L., Liu, Z. C., Liu, X. C., and Wang, J. G., 2016, Eocene Neo-Tethyan slab breakoff constrained by 45 Ma oceanic island basalt-type magmatism in southern Tibet: Geology, v. 44, no. 4, p. 283-286.

Kelly, S., Beaumont, C., and Butler, J. P., 2019, Inherited terrane properties explain enigmatic post-collisional Himalayan-Tibetan evolution: Geology, v. 48, no. 1, p. 8-14.

Ma, L., Wang, Q., Kerr, A. C., Yang, J.-H., Xia, X.-P., Ou, Q., Yang, Z.-Y., and Sun, P., 2017, Paleocene (c. 62 Ma) Leucogranites in Southern Lhasa, Tibet: Products of Syn-collisional Crustal Anatexis during Slab Roll-back?: Journal of Petrology, v. 58, no. 11, p. 2089-2114.

Nelson, K. D., Zhao, W., Brown, L. D., Kuo, J., Che, J., Liu, X., Klemperer, S. L., Makovsky, Y., Meissner, R., Mechie, J., Kind, R., Wenzel, F., Ni, J., Nabelek, J., Leshou, C., Tan, H., Wei, W., Jones, A. G., Booker, J., Unsworth, M., Kidd, W. S. F., Hauck, M., Alsdorf, D., Ross, A., Cogan, M., Wu, C., Sandvol, E., and Edwards, M., 1996, Partially Molten Middle Crust Beneath Southern Tibet: Synthesis of Project INDEPTH Results: Science, v. 274, no. 5293, p. 1684-1688.

Pilet, S., Abe, N., Rochat, L., Kaczmarek, M. A., Hirano, N., Machida, S., Buchs, D. M., Baumgartner, P. O., and Müntener, O., 2016, Pre-subduction metasomatic enrichment of the oceanic lithosphere induced by plate flexure: Nature Geoscience, v. 9, no. 12, p. 898-903.

Qi, Y., Hawkesworth, C. J., Wang, Q., Wyman, D. A., Li, Z.-X., Dong, H., Ma, T., Chen, F., Hu, W.-L., and Zhang, X.-Z., 2020, Syn-collisional magmatic record of Indian steep subduction by 50 Ma: GSA Bulletin, v. 133, no. 5-6, p. 949-962.

Romeo, I., and Álvarez-Gómez, J. A., 2018, Lithospheric folding by flexural slip in subduction zones as source for reverse fault intraslab earthquakes: Scientific Reports, v. 8, no. 1, p. 1367.

Searle, M., Simpson, R., Law, R., Parrish, R., and Waters, D., 2003, The structural geometry, metamorphic and magmatic evolution of the Everest massif, High Himalaya of Nepal–South Tibet: Journal of the Geological Society, v. 160, no. 3, p. 345-366.

Shellnutt, J. G., Bhat, G. M., Wang, K.-L., Brookfield, M. E., Jahn, B.-M., and Dostal, J., 2014, Petrogenesis of the flood basalts from the Early Permian Panjal Traps, Kashmir, India: Geochemical evidence for shallow melting of the mantle: Lithos, v. 204, p. 159-171.

Spence, D., and Turcotte, D., 1985, Magma‐driven propagation of cracks: Journal of Geophysical Research: Solid Earth, v. 90, no. B1, p. 575-580.

Vanderhaeghe, O., Laurent, O., Gardien, V., Moyen, J.-F., Gébelin, A., Chelle-Michou, C., Couzinié, S., Villaros, A., and Bellanger, M., 2020, Flow of partially molten crust controlling construction, growth and collapse of the Variscan orogenic belt: the geologic record of the French Massif Central: Bulletin de la Société Géologique de France, v. 191, no. 1, p. 25.

Vanderhaeghe, O., and Teyssier, C., 2001, Partial melting and flow of orogens: Tectonophysics, v. 342, no. 3, p. 451-472.

Wang, J.-M., Lanari, P., Wu, F.-Y., Zhang, J.-J., Khanal, G. P., and Yang, L., 2021, First evidence of eclogites overprinted by ultrahigh temperature metamorphism in Everest East, Himalaya: Implications for collisional tectonics on early Earth: Earth and Planetary Science Letters, v.

558, p. 116760.

Weinberg, R. F., 2016, Himalayan leucogranites and migmatites: nature, timing and duration of anatexis: Journal of Metamorphic Geology, v. 34, no. 8, p. 821-843.

Weller, O. M., Mottram, C. M., St-Onge, M. R., Möller, C., Strachan, R., Rivers, T., and Copley, A., 2021, The metamorphic and magmatic record of collisional orogens: Nature Reviews Earth & Environment, v. 2, no. 11, p. 781-799.

Yang, J., and Faccenda, M., 2020, Intraplate volcanism originating from upwelling hydrous mantle transition zone: Nature, v. 579, no. 7797, p. 88-91.

Yin, A., 2006, Cenozoic tectonic evolution of the Himalayan orogen as constrained by along-strike variation of structural geometry, exhumation history, and foreland sedimentation: Earth-Science Reviews, v. 76, no. 1, p. 1-131.

Yuan, C., Zhou, M.-F., Sun, M., Zhao, Y., Wilde, S., Long, X., and Yan, D., 2010, Triassic granitoids in the eastern Songpan Ganzi Fold Belt, SW China: magmatic response to geodynamics of the deep lithosphere: Earth and Planetary Science Letters, v. 290, no. 3-4, p. 481-492.

Zeng, L., Gao, L.-E., Xie, K., and Liu-Zeng, J., 2011, Mid-Eocene high Sr/Y granites in the Northern Himalayan Gneiss Domes: melting thickened lower continental crust: Earth and Planetary Science Letters, v. 303, no. 3, p. 251-266.

Zhao, J., Yuan, X., Liu, H., Kumar, P., Pei, S., Kind, R., Zhang, Z., Teng, J., Ding, L., and Gao, X., 2010, The boundary between the Indian and Asian tectonic plates below Tibet: Proceedings of the National Academy of Sciences, v. 107, no. 25, p. 11229-11233.

Zheng, Y.-c., Hou, Z.-q., Fu, Q., Zhu, D.-C., Liang, W., and Xu, P., 2016, Mantle inputs to

Himalayan anatexis: Insights from petrogenesis of the Miocene Langkazi leucogranite and its dioritic enclaves: Lithos, v. 264, p. 125-140.

Zhu, D.-C., Wang, Q., Chung, S.-L., Cawood, P. A., and Zhao, Z.-D., 2019, Gangdese magmatism in southern Tibet and India–Asia convergence since 120 Ma: Geological Society, London, Special Publications, v. 483, no. 1, p. 583-604.

Zhu, D.-C., Zhao, Z.-D., Niu, Y., Dilek, Y., Hou, Z.-Q., and Mo, X.-X., 2013, The origin and pre-Cenozoic evolution of the Tibetan Plateau: Gondwana Research, v. 23, no. 4, p. 1429-1454.

Figure 1. (a) Simplified geologic map of the Himalayan orogenic belt, southern Tibet (after Zeng et al., 2011) showing locations of the magmatism and metamorphism in the northern Himalaya, as well as the location of the study area. Locations and ages of Eocene magmatism in Tethyan Himalaya are listed in Table DR1. YZS: Yarlung Zangbo suture; STDS: Southern Tibet Detachment System; MCT: Main Central Thrust; MBT: Main Boundary Thrust; LH: Lower Himalaya. (b) Geological map of the study area. (c) Histogram of ages for Eocene magmatic rocks in the Tethyan Himalaya. The convergence rate of Indian continent is shown as green dotted line. The dark blue line shows the kernel density estimate (Chapman and Kapp, 2017) for the age of the southern Lhasa magmatism. (d) Plots of representative pressure-temperature (P-T) and thermal gradients for Cenozoic metamorphism in the Himalaya. The data and references are listed in Table DR5.

Figure 2. Geochemistry and Tera-Wasserburg diagram of the Gyantse dikes. The Langshan gabbro data are from Ji et al. (2016). The data for Tethyan MORB, Panjal basalt, Eocene granite and Oligo-Miocene leucogranite shown in Table DR6. Langshan gabbro (12FW63, $[^{87}Sr/^{86}Sr]_i$ = 0.706571, $\varepsilon_{Nd}(t)$ =5.8) and Panjal low-Ti basalt (PJ2-014, $[^{87}Sr/^{86}Sr]_i$ = 0.712667, $\varepsilon_{Nd}(t)$ = -6.4) represent the asthenospheric and lithospheric mantle end-members for modeling, respectively. The numbers along the blue tick-line indicate percentage contribution of asthenosphere material. MSWD = mean square of weighted deviation.

Figure 3. Schematic diagram illustrating the formation of the Eocene (ca. 50-35 Ma) orogen-parallel magmatic and metamorphic zone in the Tethyan Himalaya due to lithospheric flexure. Mafic melts from the lithosphere-asthenosphere boundary percolate into the Indian continental lithosphere and underplate the continental crust along fractures, causing coeval orogen-parallel thickened crustal anatexis. The steepening subduction of Neo-Tethyan and Indian lithosphere resulted in the subduction channel widening and asthenospheric upwelling and/or a slab break-off, causing melting to produce coeval magmatism in the Lhasa block. (b) Elevation and S-wave receiver function profiles along the dark blue dotted line in Fig.1a, are adapted from Zhao et al. (2010). The blue low velocity zone indicates a possible partial melting zone.

Figure 1

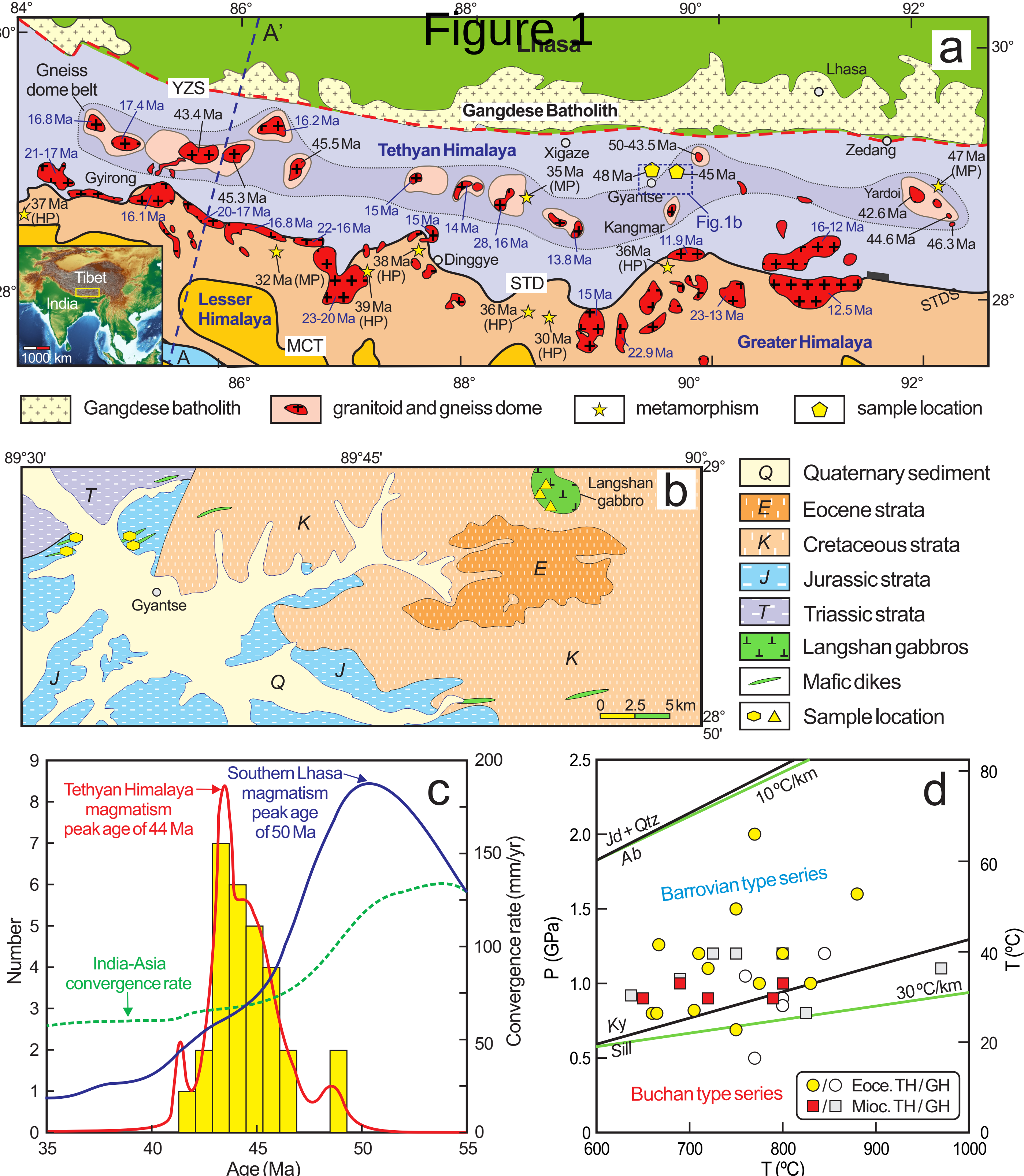
84°
86°
88°
90°
92°
30°
28°
a
Lhasa
A'
A
Gneiss dome belt
YZS
Gangdese Batholith
Tethyan Himalaya
Lhasa
Xigaze
Zedang
Gyirong
Gyantse
Kangmar
Dinggye
Yardoi
Fig.1b
STD
MCT
STDS
Lesser Himalaya
Greater Himalaya
Tibet
India
1000 km
16.8 Ma
17.4 Ma
43.4 Ma
16.2 Ma
45.5 Ma
21-17 Ma
45.3 Ma
20-17 Ma
16.1 Ma
16.8 Ma
22-16 Ma
37 Ma (HP)
32 Ma (MP)
15 Ma
15 Ma
14 Ma
28, 16 Ma
35 Ma (MP)
50-43.5 Ma
48 Ma
45 Ma
13.8 Ma
38 Ma (HP)
39 Ma (HP)
23-20 Ma
36 Ma (HP)
30 Ma (HP)
15 Ma
22.9 Ma
36Ma (HP)
11.9 Ma
16-12 Ma
23-13 Ma
12.5 Ma
47 Ma (MP)
42.6 Ma
44.6 Ma
46.3 Ma
Gangdese batholith
granitoid and gneiss dome
metamorphism
sample location
89°30'
89°45'
90°
29°
28° 50'
b
Langshan gabbro
T
K
E
J
Q
Gyantse
0 2.5 5 km
Q Quaternary sediment
E Eocene strata
K Cretaceous strata
J Jurassic strata
T Triassic strata
Langshan gabbros
Mafic dikes
Sample location
c
Tethyan Himalaya magmatism peak age of 44 Ma
Southern Lhasa magmatism peak age of 50 Ma
India-Asia convergence rate
Number
Convergence rate (mm/yr)
Age (Ma)
d
Jd + Qtz
Ab
10 °C/km
Barrovian type series
Ky
Sill
30 °C/km
Buchan type series
Eoce. TH / GH
Mioc. TH / GH
P (GPa)
T (°C)

Figure 2

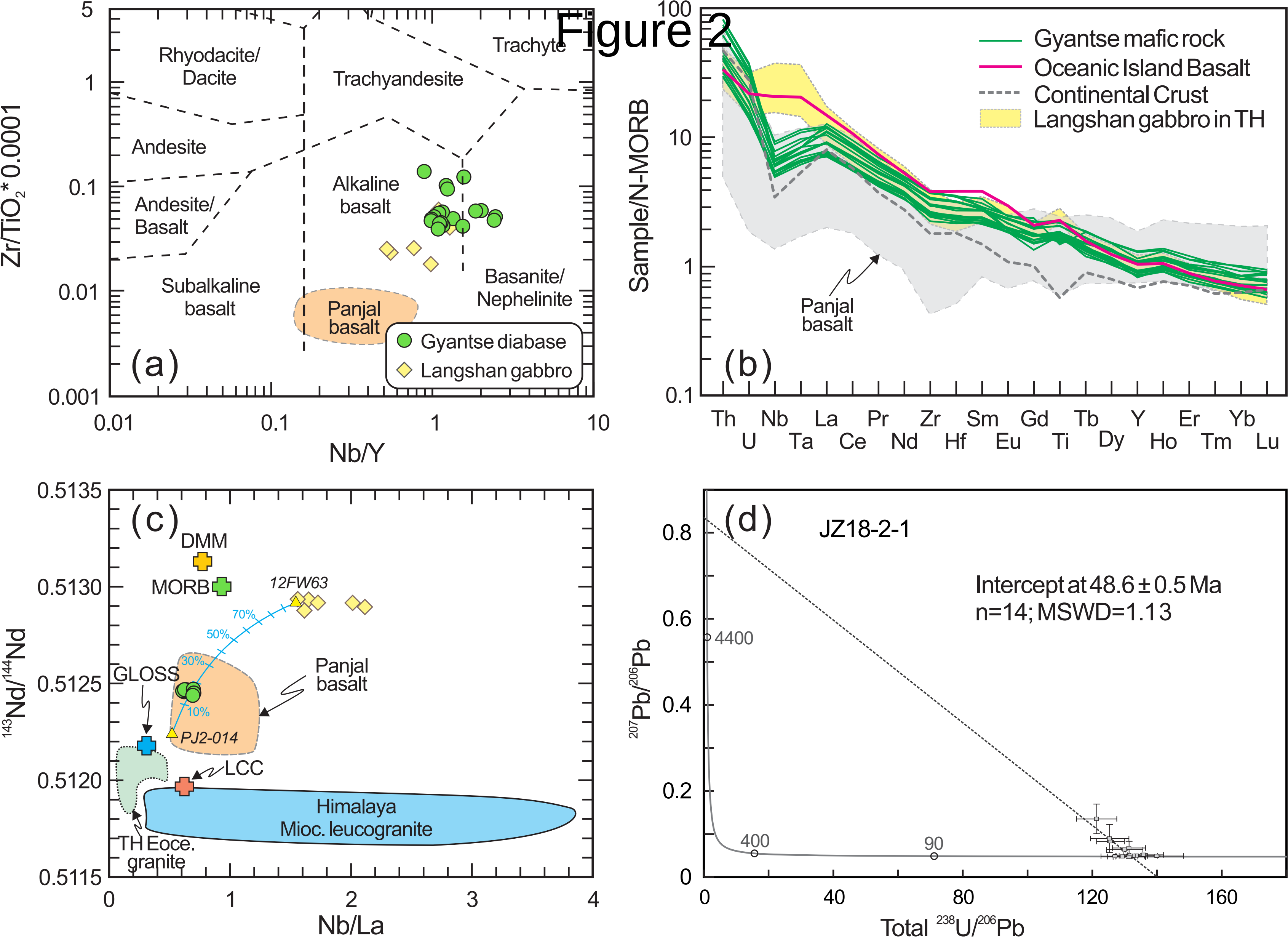

Rhyodacite/
Dacite
Trachyte
Trachyandesite
Andesite
Andesite/
Basalt
Alkaline
basalt
Subalkaline
basalt
Basanite/
Nephelinite
Panjal
basalt
(a)
Gyantse diabase
Langshan gabbro
Zr/TiO2*0.0001
Nb/Y
Gyantse mafic rock
Oceanic Island Basalt
Continental Crust
Langshan gabbro in TH
Sample/N-MORB
Panjal
basalt
(b)
Th U Nb Ta La Ce Pr Nd Zr Hf Sm Eu Gd Ti Tb Dy Y Ho Er Tm Yb Lu
(c)
DMM
MORB
12FW63
70%
50%
30%
10%
GLOSS
PJ2-014
Panjal
basalt
LCC
Himalaya
Mioc. leucogranite
TH Eoce.
granite
143Nd/144Nd
Nb/La
(d)
JZ18-2-1
Intercept at 48.6 ± 0.5 Ma
n=14; MSWD=1.13
4400
400
90
207Pb/206Pb
Total 238U/206Pb

Figure 3

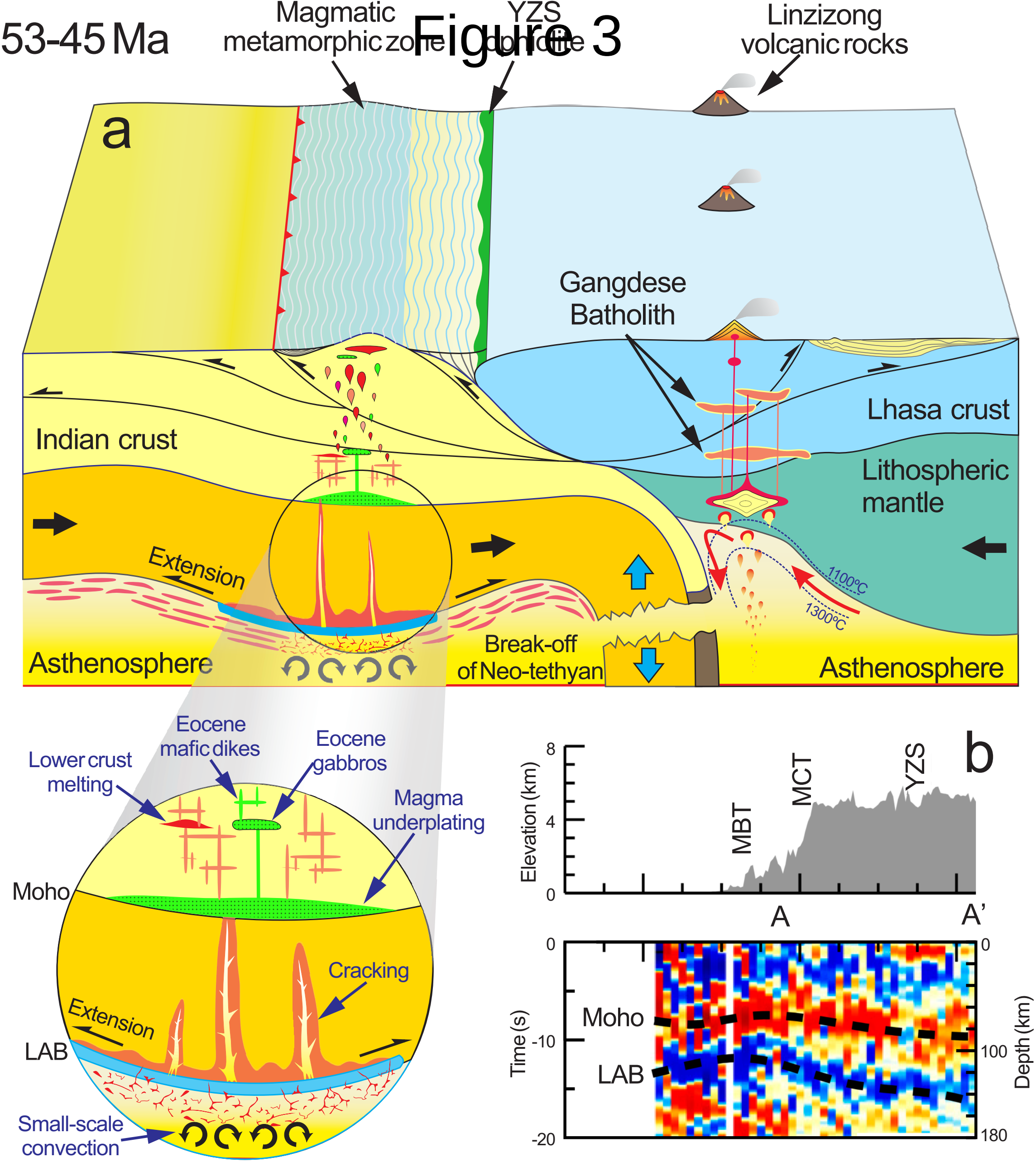
53-45 Ma
Magmatic metamorphic zone
YZS ophiolite
Linzizong volcanic rocks
a
Gangdese Batholith
Lhasa crust
Indian crust
Lithospheric mantle
Extension
1100°C
1300°C
Asthenosphere
Break-off of Neo-tethyan
Asthenosphere
Lower crust melting
Eocene mafic dikes
Eocene gabbros
Magma underplating
Moho
Cracking
Extension
LAB
Small-scale convection
b
Elevation (km)
MBT
MCT
YZS
A
A'
Moho
LAB
Time (s)
Depth (km)